Influence of enhanced Asian NO$_x$ emissions on ozone in the Upper Troposphere and Lower Stratosphere (UTLS) in chemistry climate model simulations

Chaitri R.[1], Suvarna Fadnavis[1*], Rolf Müller[2], Ayantika D. C.[1], Felix Ploeger[2], Alexandru Rap[3]

[1]Indian Institute of Tropical Meteorology, Pune, India

[2]Forschungszentrum Jülich GmbH, IEK7, Jülich, Germany

[3]School of Earth and Environment, University of Leeds, Leeds, United Kingdom

*Email of corresponding author: suvarna@tropmet.res.in

Abstract:

The Asian summer monsoon (ASM) anticyclone is the most pronounced circulation pattern in the Upper Troposphere and Lower Stratosphere (UTLS) during the Northern Hemisphere summer. Asian summer monsoon convection plays an important role in efficient vertical transport from the surface to the upper-level anticyclone. In this paper we investigate the potential impact of enhanced anthropogenic nitrogen oxides (NO$_x$) on the distribution of ozone in the UTLS using the fully-coupled aerosol chemistry climate model, ECHAM5-HAMMOZ. Ozone in the UTLS is influenced both by the convective uplift of ozone precursors and by the uplift of enhanced NO$_x$ induced tropospheric ozone anomalies. We performed anthropogenic NO$_x$ emission sensitivity experiments over India and China. In these simulations, covering the years 2000-2010 anthropogenic NO$_x$ emissions have been increased by 38% over India and by 73% over China with respect to the emission base year 2000. These emission increases are comparable to the observed linear trends of 3.8 % per year over India and 7.3% per year over China during the period 2000 to 2010. Enhanced NO$_x$ emissions over India by 38 % and China by 73 % increase the ozone radiative forcing in the ASM Anticyclone (15º-40°N, 60º-120°E) by 16.3 mW m^{-2} and 78.5 mW m^{-2} respectively. These elevated NO$_x$ emissions produce significant warming over the Tibetan Plateau and increase precipitation over India due to a strengthening of the monsoon Hadley

25   circulation.

26   However increase in NO_x emissions over India by 73% (similar to the observed increase over China),

27   results in large amount of ozone production over the Indo Gangetic plain and Tibetan Plateau. The

28   higher ozone concentrations, in turn, induce a reversed monsoon Hadley circulation and negative

29   precipitation anomalies over India. The associated subsidence suppresses vertical transport of NO_x and

30   ozone into the ASM anticyclone.

31   Key words: Asian summer monsoon, Tropospheric ozone, Tropospheric NO_x, NO_x transport, Upper

32   troposphere and lower stratosphere, Ozone radiative forcing.

34   **1. Introduction**

35   Rapid economic development and urbanization in Asia has resulted in an unprecedented growth in

36   anthropogenic emissions of nitrogen oxides (NO_x), carbon monoxide (CO), carbon dioxide (CO_2),

37   methane (CH_4). Many of these species affect concentrations of tropospheric ozone, which is both an

38   important polluting agent and a greenhouse gas (Wild and Akimoto, 2001; Chatani et al 2014; Revell et

39   al., 2015). Ground based and satellite observations show a large amount of these ozone precursors

40   concentrated over India and China (Sinha et al., 2014; Richter et al., 2005; Jacob et al., 1999; Zhao et

41   al., 2013; Gu et al., 2014). Studies show that tropospheric ozone production over Asia is controlled by

42   the abundance of NO_x and VOCs (Sillman, 1995, Lei et al., 2004, Zhang et al., 2004 and Tie et al.,

43   2007), with large regions such as India and China being NO_x limited regions. Therefore, increased NO_x

44   in these regions leads to an increase in ozone concentrations (Yamaji et al., 2006; Sinha et al., 2014;

45   Fadnavis et al., 2014). Recently, positive trends in Asian tropospheric column NO_2 have been reported,

46   i.e. 3.8 % yr^{-1} over India, using SCanning Imaging Absorption SpectroMeter for Atmospheric

47   CHartographY (SCIAMACHY) observations for the period 2003-2011 (Ghude et al., 2013), and 7.3%

48   yr^{-1} over China using Ozone Monitoring Instrument (OMI) observations for the period 2002-2011

49 (Schneider and van der A., 2012). Lightning contributes to the production of NOx in the middle and

50 upper troposphere (Barret et al, 2016). Over the Asian region, lightning contributes ~40% to NO_x and

51 20% to ozone production in the middle and upper troposphere during the monsoon season (Tie et al.

52 2001; Fadnavis et al. 2015). The upper tropospheric ozone concentration is determined by in-situ

53 production from both lightning and ozone precursors which are transported from the boundary layer

54 (Søvde et al., 2011; Barret et al, 2016).

55   Tropospheric ozone has a warming effect on climate, its estimated radiative forcing due to

56 increased concentrations since pre-industrial times being $0.4 \, \mathrm{W \, m^{-2}}$, with a 5 to 95% confidence range

57 of (0.2 to $0.6 \, \mathrm{W \, m^{-2}}$) (Stevenson et al., 2013; Myhre et al., 2013). Previous studies highlighted the

58 importance of the tropical tropopause region for ozone radiative forcing (Lacis et al, 1990; Riese et al.,

59 2012; Rap et al., 2015) and showed that ozone perturbations exert a large influence on the thermal

60 structure of the atmosphere (e.g., Thuburn and Craig, 2002; Foster and Shine 1997). A recent study

61 based on Atmospheric Chemistry and Climate Model Intercomparison Project (ACCMIP) models

62 reported that NO_x and CH_4 are the greatest contributors in determining tropospheric ozone radiative

63 forcing (Stevenson et al., 2013).

64   Asian Summer Monsoon (ASM) convection efficiently transports Asian pollutants from the

65 boundary layer into the Upper Troposphere and Lower Stratosphere (UTLS) (Randel and Park, 2006;

66 Randel et al. 2010; Fadnavis et al., 2013, 2015). Studies pertaining to modeling and trajectory analysis

67 confirm this finding (Li et al., 2005; Park et al., 2007; Randel et al., 2010; Chen et al., 2012; Vogel et

68 al., 2015, 2016). Satellite observations show the confinement of a number of chemical constituents like

69 water vapor (H_2O), CO, CH_4, ethane, hydrogen cyanide (HCN), PAN and aerosols, within the ASM

70 anticyclone (Park et al., 2004, 2007, 2008; Li et al., 2005; Randel and Park, 2006; Xiong et al., 2009;

71 Randel et al. 2010; Lawrence et al., 2011; Abad et al., 2011; Fadnavis et al., 2013;2014;2015; Barret et

72 al., 2016) which has potential implications on stratospheric chemistry and dynamics. Thus the rise in

anthropogenic emissions over the ASM region alters the chemical composition of the UTLS (Lawrence et al., 2011; Fadnavis et al, 2014, 2015) during the monsoon season. Another prominent feature of the satellite observations is an ozone minimum in the ASM anticyclone (near 100 hPa) (Gettelman et al., 2004; Konopka et al., 2010; Braesicke et al., 2011). This ozone minimum is linked to upward transport of ozone poor air masses (Gettelman et al., 2004; Park et al., 2007; Kunze et al., 2010). Observations show that convectively lifted air masses arriving in the anticyclone are ozone poor but rich in ozone precursors. Balloon sonde observations show that ozone variations near the anticyclone are strongly correlated with temperature near the tropopause (Tobo et al., 2008). Thus the linkage of low ozone and high concentrations of ozone precursors with the temperature variation in the anticyclone is an open question.

In this study we ask the question 'how do increasing Asian NO_X emissions and the associated ozone production affect ozone radiative forcing and monsoon circulation?'. We perform sensitivity experiments of increased anthropogenic NO_x emissions using the state-of-the-art ECHAM5-HAMMOZ (European Centre General Circulation Model version5) chemistry climate model (Roeckner et al., 2003; Horowitz et al., 2003; Stier et al., 2005). We estimate the ozone radiative forcing for the different anthropogenic NO_x emission scenarios, together with associated changes in temperature and the monsoon circulation. The paper is organized as follows: in Section 2 the data and model set up are described;the results are summarized in Section 3 and discussed in Section 4, followed by conclusions given in Section 5.

2. Data description and Model setup

2.1 Satellite measurements

Earth Observing System (EOS) microwave limb sounder (MLS) is one of the four instruments on the NASA's EOS Aura satellite flying in the polar sun-synchronous orbit. It measures the thermal

emissions at millimeter and sub millimeter wavelengths (Waters et al., 2006). It performs 240 limb

scans per orbit with a footprint of ~6 km across-track and ~200 km along-track, providing ~3500

profiles per day. MLS also measures vertical profiles of temperature, ozone, CO, H_2O, and many other

constituents in the mesosphere, stratosphere and upper troposphere (Waters et al., 2006). In the UTLS,

MLS has a vertical resolution of about 3 km. MLS vertical profiles of ozone show good agreements

with the Stratospheric Aerosol and Gas Experiment II (SAGE-II), Halogen Occultation Experiment

(HALOE), Atmospheric Chemistry Experiment (ACE) and ozonesonde measurements (Froidevaux et

al.,2006). The MLS ozone profiles are considered to be useful in the range of 215 – 0.46 hPa (Livesey

et al., 2005). In this study we analyze the MLS level 2 (version 4) ozone mixing ratios data for the

period 2004 – 2013. The data has been interpolated to potential temperature levels and gridded

horizontally, within latitude bins of equal area (with the equatorial bin of 150km width) and longitude

bins of about 8.5 degrees. This data can be accessed from http://mls.jpl.nasa.gov/. For comparison,

simulated ozone is convolved with the MLS averaging kernel (Livesey et al. 2011).

2.2 Model simulation and experimental setup

We employ the aerosol-chemistry-climate model ECHAM5-HAMMOZ which comprises the

general circulation model ECHAM5 (Roeckner et al., 2003), the tropospheric chemistry module,

MOZART2 (Horowitz et al 2003) and the aerosol module, Hamburg aerosol model (HAM) (Stier et al.,

2005). It includes NO_x, VOC and aerosol chemistry. The gas phase chemistry is based on the chemical

scheme provided by the MOZART-2 model (Horowitz et al., 2003) which includes detailed chemistry

of the O_x-NO_x hydrocarbon system with 63 tracers and 168 reactions. The $O(^1D)$ quenching reaction

rates used are taken from Sander et al., (2003) and isoprene nitrates chemistry taken from Fiore et al.,

(2005). The dry deposition in ECHAM5-HAMMOZ follows the scheme given by Ganzeveld and

Lelieveld (1995). Soluble trace gases like HNO_3 and SO_2 are also subject to wet deposition. In-cloud

and below-cloud scavenging follows the scheme given by Stier et al. (2005). Interactive calculation of cloud droplet number concentration is according to Lohmann et al (1999) and ice crystal number concentrations are according to Kärcher and Lohmann (2002). The convection scheme is based on the mass flux scheme developed by Tiedke (1989).

The model is run at a T42 spectral resolution corresponding to about 2.8°×2.8° in the horizontal dimension and 31 vertical hybrid σ – p levels from the surface to 10 hPa. In our model simulations, emissions from anthropogenic sources and biomass burning are from the year 2000 RETRO project data set (available at http://eccad.sedoo.fr/) (Schultz et al., 2004; 2005; 2007; 2008). Emissions of SO_2, BC and OC are based on the AEROCOM-II emission inventory, also for the year 2000 (Dentener et al., 2006). The distribution of NO_x emission mass flux (kg m^{-2} s^{-1}) averaged for the Asian summer monsoon season (June–September) is shown in Supplementary Fig. S1. It shows high values over the Indo Gangetic Plains and East China. Other details of model parameterizations, emissions and evaluation are described by Fadnavis et al. (2013; 2014; 2015) and Pozzoli et al. (2008a, b; 2011). Each of our model experiments consists of continuous simulations for eleven years from 2000 to 2010. The base year for emissions is taken as 2000 and emissions were repeated every year throughout the simulation period. Meteorology varied due to varying monthly mean sea surface temperature (SST) and sea ice concentration (SIC). The AMIP2 SSTs and SIC varying for the period 2000 – 2010 were specified as a lower boundary condition.

In order to understand the impact of enhanced anthropogenic NO_x emissions on the distribution of ozone in the UTLS, sensitivity simulations were performed for the period 2000 – 2010. The experimental set up is the same as described by Fadnavis et al., (2015). The four simulations analyzed in this study are: (1) a reference experiment (CTRL) and three sensitivity experiments (referred to as experiments 2 - 4), where the anthropogenic NO_x emissions over India and China are scaled in accordance with the observed trends. In experiment (2), anthropogenic NO_x emissions are increased

over India by 38% (Ind38), in experiment (3) increases over China by 73% (Chin73) are prescribed. In order to analyze the effects of similar NO_x percentage increases over India and China, NO_x emissions are increased over India by 73% (Ind73) in experiment (4). The emission perturbations were obtained from observed NO_2 trends of 3.8% per year over India (Ghude et al., 2013) and 7.3% per year over China (Schneider and van der A., 2012). Hiboll et al. (2013) also reported similar increasing NO_x values over megacities in India and China. All four simulations use the same VOC and CO emissions and they all include NO_x production due to lightning (lightning-on) and soil emissions (see Table 1, showing details pertaining to these experiments). Therefore NO_x or ozone anomalies obtained from difference between Ind38, Ind73 and Chin73 with respective to CTRL simulation do not have an impact of lightning or soil emissions as they are same in all the simulations.

In addition, a series of four lightning-off simulations were performed for the same period and boundary conditions as experiments 1-4 (these simulations are the same as the ones documented by Fadnavis et al. (2015))The impact of lightning on NO_x production is estimated by comparing the CTRL (lightning-on) simulation with lightning-off simulations.

The accuracy of the simulation of the monsoon circulation will likely depend on the model resolution and increased vertical resolution may improve the model performance (Druyan et al., 2008; Abhik et al., 2014). While we acknowledge the limitations of our relatively course vertical resolution (dictated by our computational resources), the model is still capable of reasonably simulating the general regional spatial pattern of precipitation and low-level circulation (Rajeevan et al., 2005) (see Supplementary Fig. S2, showing simulated seasonal mean precipitation and circulation at 850 hPa in the CTRL simulation).

The heating rates and radiative forcings associated with the ozone changes in our three sensitivity simulations are calculated using the Edwards and Slingo (1996) radiative transfer model and the fixed dynamical heating approximation for stratospheric temperature adjustment. Similarly to

170 previous studies (Riese et al., 2012; Bekki et al., 2013; Rap et al., 2015), we used the off-line version of

171 the model, with six shortwave and nine longwave bands, and a delta-Eddington 2-stream scattering

172 solver at all wavelengths.

173

174 **3. Results**

175 **3.1 Comparison with MLS satellite measurements in the UTLS**

176 The spatial distributions of ozone mixing ratios from MLS observations at 100 hPa and from

177 the CTRL ECHAM5-HAMMOZ simulation at 90 hPa (the nearest model level) after smoothing with

178 the averaging kernel of MLS are illustrated in Fig. 1a and Fig. 1b, respectively. The climatological

179 horizontal winds plotted in the figure clearly show the anticyclonic upper level monsoon circulation.

180 Recent attempts to characterize the extent of the anticyclone are based either on potential vorticity on

181 isentropic surfaces or geopotential height on pressure surfaces. Here we apply both characterizations of

182 the anticyclone and show the PV contour related to the maximum PV gradient on 380K (calculated

183 from ERA-Interim reanalysis following Ploeger et al., 2015), and the 270m geopotential height

184 anomaly as proposed by Barret et al. (2016). The close agreement of both methods shows that from a

185 climatological point of view the two criteria yield a very similar picture of the anticyclonic circulation

186 and the related trace gas confinement. Locally and at particular dates, however, differences may be

187 larger with potential vorticity correlating better with confined trace gas anomalies than geopotential

188 height (e.g., Garny and Randel, 2013; Ploeger et al., 2015). The spatial pattern of low ozone

189 concentrations in the monsoon anticyclone is well simulated in the model. It is in good agreement with

190 MLS (90-140 ppbv), MIPAS (80-120 ppbv) and SAGE II (<150ppbv) measurements (Kunze et al.,

191 2010; Randel et al., 2001; Randel and Park 2006; Park et al., 2007).

192 Vertical profiles of ozonesonde measurements (averaged for the monsoon season during 2001-

193 2009) at Indian stations, Delhi (28.61ºN, 77.23ºE), Pune (18.52ºN, 73.85ºE) and Thiruvananthapuram

194   (8.48ºN, 76.95E) are compared with MLS measurements and ECHAM5-HAMMOZ simulated ozone

195   mixing ratios in Figs. 1(c)-(e). ECHAM5-HAMMOZ simulations show good agreement with MLS data

196   between 200 hPa and 50 hPa at all three stations. Comparison of ozonesonde observations with the

197   ECHAM5-HAMMOZ simulation shows reasonably good agreement at Pune, compared to Delhi and

198   Thiruvananthapuram where there are some discrepancies. The simulated ozone mixing ratios are lower

199   than ozonesonde measurements by 10-40 ppb between 500 – 90 hPa at Pune and by ~70-90 ppb in the

200   upper troposphere (500-150 hPa) at Delhi. At Thiruvananthapuram, while at altitudes below 375 hPa,

201   simulated ozone mixing ratios show good agreement with ozonesonde data, at the altitudes above 375

202   hPa, simulated values are lower than observations by ~20-70 ppb. The differences between model and

203   ozonesonde data may be due to different grid sizes: the ECHAM5-HAMMOZ model grid size is ~280

204   km, while balloon observations are within ~30-180 km spatial range (balloon typically drifts ~30–180

205   km horizontally). In addition, previous work comparing these model simulations with various aircraft

206   observations during the monsoon season, found a reasonable agreement for PAN, NO_x, HNO_3 and O_3

207   mixing ratios (Fadnavis et al., 2015).

208

209   **3.2 Transport of enhanced NO_x emissions into the UTLS**

210   Recent satellite observations and model simulations quantified the impact of convective

211   transport of boundary layer pollution into the ASM anticyclone during the Asian summer monsoon

212   season (Gettelman et al., 2004; Randel et al., 2010; Fadnavis et al., 2013, 2014, 2015). These pollutants

213   are further transported across the tropopause as evident in satellite observations of, e.g. water vapour

214   (Bian, 2012), hydrogen cyanide (HCN) (Randel, 2010), CO (Schoeberl et al., 2006), Peroxyacetyl

215   nitrate (PAN) (Fadnavis et al.,2014; 2015), aerosols (Vernier et al., 2015, Fadnavis et al., 2013). To

216   understand the influence of monsoon convection on the vertical distribution of NO_x we show zonal and

217   meridional cross sections over India and China. Vertical distributions of NO_x averaged for the monsoon

season over Indian latitudes (8°N-35°N), and Chinese latitudes (20°N-45°N) as obtained from CTRL simulations are shown in the Supplementary Figs. S3(a) and S3(b) respectively. These figures show elevated levels of NO_x extending from the surface to the upper troposphere over India and China. The wind vectors along with the distribution of cloud droplet number concentration (CDNC) and ice crystal number concentration (ICNC), (Supplementary Figs. S4(a), S4(b) and S4(c)) indicate strong convective transport from the Bay of Bengal (BOB), South China Sea and southern slopes of Himalayas which might lift the boundary layer NO_x to the upper troposphere.

During the monsoon season, the NO_x distribution in the UTLS is also influenced by lightning, in addition to transport from anthropogenic sources. Lightning activity during this season was found to be more pronounced in Asia, compared to the other monsoon regions such as North America, South America and Africa (Ranalkar and Chaudhari, 2009; Penki and Kamra, 2013). In our simulations, we find that lightning produces 40-70% of NO_x over north India and Bay of Bengal and 40-60% over the Tibetan Plateau and West China region (Supplementary Fig. S5).

Fig. 2 shows the vertical distribution of anthropogenic NO_x anomalies obtained from the Ind38, Ind73, Chin73 simulations, compared with the CTRL simulation. Ind38 and Chin73 simulations show that the convective winds over the Bay of Bengal (80-90°E) (Figs. 2(a) and 2(c)) and at the southern flank_of the Himalayas (Figs. 2(d) and 2(f)) lift up the enhanced NO_x emissions to the upper troposphere (UT). While most transport is mainly into the UT, parts of it also occur into the lower stratosphere, with cross tropopause transport being particularly evident in the Chin73 simulation (Figs. 2(c) and 2(f)). Randel and Park (2006) and Randel et al. (2010) also reported that pollution transported by Asian monsoon convection enters the stratosphere. Our results are also in good agreement with previous studies indicating significant vertical transport due to strong monsoon convection from the southern slopes of Himalayas (Fu et al., 2006, Fadnavis et al., 2013; 2014) and the South China Sea (Park et al 2009; Chen et al., 2012). In the upper troposphere, NO_x is transported over Iran and Saudi

242   Arabia along the descending branch of the large scale monsoon circulation (Rodwell and Hoskins,

243   1995). However, the cross tropopause transport is not present in the Ind73 simulation, where it is

244   inhibited by the wind anomalies that show a descending branch over central India (~20°N, 75°E) (Figs.

245   2(b) and 2(e)). These descending wind anomalies may also be related to the associated ozone radiative

246   forcing and temperature changes, as discussed in Section 4.

247

248   **3.3 Impact of enhanced anthropogenic NO_x on the tropospheric ozone distribution**

249   We calculate the change in ozone production over India and China due to enhanced NO_x

250   emissions in the Ind38, Ind73 and Chin73 simulations with respect to the CTRL simulation. Figure 3,

251   showing longitude-pressure cross sections of net ozone production (ppt/day) changes, indicates that the

252   majority of this additional ozone production occurs in the lower troposphere. At altitudes below 300

253   hPa, the ozone production and loss vary between -15 ppt day^{-1} and 15 ppt day^{-1}. In the upper

254   troposphere (300-150 hPa), the estimated amount of additional net ozone production in Ind38 and

255   Ind73 simulation is 3-7 ppt day^{-1}, while in the Chin73 simulation it is ~3-13 ppt day^{-1}. We also simulate

256   ozone loss near the tropopause in the Ind73 simulation (Figure 3b). We note that these ozone anomalies

257   are not driven by lightning NO_x, as this is included in all simulations. It is interesting to understand

258   ozone production over the highly populated Indo Gangetic Plain and Tibetan Plateau region. A

259   longitude pressure cross section over this region show that ozone production over the Indo Gangetic

260   Plain and Tibetan Plateau in Ind73 is (20-25ppt/day) is much larger than Ind38 (6-20 ppt/day) in the

261   lower troposphere (Supplementary Fig. S6).

262   Figure 4 shows the vertical distribution of ozone anomalies induced by enhanced anthropogenic

263   NO_x emissions in the three perturbation experiments compared to the CTRL simulation, averaged over

264   India and China. Although the air mass in the monsoon anticyclone is relatively poor in ozone

265   (Fig.1(b)), the elevated amounts of ozone anomalies in response to enhanced anthropogenic NO_x

266   emissions are clearly seen in Fig. 4. This may be partially due to convective transport of enhanced-

267   NO_x-emission induced ozone anomalies produced in the lower troposphere, and partially due to

268   chemical ozone production from convectively transported boundary layer ozone precursors. Ozone

269   anomalies are enhanced near 300-200 hPa over west Asia (40-60ºE) (Figs. 4a-c), possibly due to the

270   vertical convective transport of ozone anomalies and precursors and also from subsequent horizontal

271   transport in the monsoon anticyclone (Barret et al., 2016).

272   Latitude-pressure cross sections of enhanced-NO_x-emission induced ozone anomalies plotted in

273   Figs. 4(d) and 4(f) illustrate how convection over the Bay of Bengal, the southern slopes of the

274   Himalayas and the South China Sea lifts the enhanced ozone anomalies from India and China into the

275   upper troposphere. These ozone anomalies are also transported further across the tropopause and into

276   the lower stratosphere, where ozone production is also driven by photolysis and NO_x anomalies.

277   In the Ind73 simulation, similarly to the NO_x anomaly distribution (Figs. 2(b) and 2(e)), the

278   descending branch of circulation over central India also suppresses the vertical transport of ozone

279   anomalies across the tropopause (Figs. 4(b) and 4(e)). This subsidence may be related to ozone heating

280   rate changes, as there is significant increase in ozone production over the Indo Gangetic plain and

281   Tibetan Plateau in the lower troposphere due to enhanced anthropogenic NO_x emissions (Section 4).

282

283   **3.4 Distribution of NO_x and ozone in the anticyclone**

284   The distributions of NO_x and ozone anomalies in the monsoon anticyclone region in the Ind38,

285   Ind73 and Chin73 simulations with respect to the CTRL simulation are shown in Figs. 5(a)-(f). A

286   maximum in the NO_x anomalies in the ASM anticyclone (60°E to 120°E) is seen in all the simulations.

287   NO_x anomalies are high at the eastern part of the monsoon anticyclone since convective injection into

288   the anticyclone occurs mainly in that region (Fadnavis et al., 2013). Increase in NO_x anomalies in the

289   Ind38 simulation is higher (Fig. 5(a)) than that in the Ind73 simulation (Figs. 5(b)), mainly due to

descending motion over central India in the Ind73 simulation, as seen in the previous sections. In contrast to NO_x anomalies, ozone anomalies in Ind38 are lower than Ind73, especially in the north-eastern part of anticyclone. Satellite observations also show high ozone precursors and low ozone amounts in the anticyclone (Park et al., 2007; Barret et al., 2016). Similarly, the Chin73 simulation shows higher values of NO_x anomalies (>18%) and strong negative ozone anomalies (~-8%) in the north eastern region of the monsoon anticyclone (Figs. 5(c) and 5(f)). Figure 5 also shows that the tropical easterly jet transports NO_x and ozone (from India and China) to Saudi Arabia, Iran and Iraq.

4. Discussion

To estimate the radiative impact of the simulated ozone changes, we use the offline version of the Edwards and Slingo (1996) radiative transfer model. Figure 6 shows the radiative forcing caused by the ozone changes in each of the three sensitivity simulations compared to the CTRL simulation. The overall increase in tropospheric ozone (see Figure 4) has a warming effect on climate, with the regional average radiative forcing in the monsoon anticyclone (15ºN-40ºN, 60-120ºE) estimated at16.3 mW m^{-2}, 69.9 mW m^{-2}, and 78.5 mW m^{-2} in the Ind38, Ind73, and Chin73 simulations, respectively.

We also investigate the impact on the atmospheric heating rates caused by the ozone changes. Figure 7 shows the zonal mean heating rate anomalies for the Ind38, Ind73 and Chin73 simulations, compared to the CTRL simulation. These three simulations show positive and negative heating rates anomalies between 400-200 hPa. However, in the upper troposphere and lower stratosphere (200-50 hPa) ozone heating rates are negative over Indo Gangetic plain (20-30°N) and Tibetan Plateau (30-40ºN) region. In Ind73 simulation, ozone heating rate anomalies are positive in the lower troposphere over the Indo Gangetic plain (1000-750 hPa) and Tibetan plateau (600-400 hPa). This may be due to large amount of ozone production in the lower troposphere over these regions (Fig. S6). This heating may produce changes in the circulation leading to ascending motion over the Tibetan Plateau and a

descending branch over central India (~20ºN), i.e. a reversal of monsoon Hadley circulation (Fig. 9(b)).

Figures 8 shows latitude pressure cross-section of temperature anomalies (K) obtained from Ind38, Ind73 and Chin73 simulations. Ind38 and Chin73 simulations show anomalous warming in the upper troposphere over the Tibetan Plateau while it is subdued in the Ind73 simulation. Upper tropospheric warming over the Tibetan plateau is one of the key factors responsible for the ASM circulation (Flohn 1957; Yanai et al., 1992; Meehl, 1994; Li and Yanai, 1996; Wu and Zhang, 1998). Flohn (1957, 1960) suggested that upper tropospheric warming over the Tibetan plateau leads to increased Indian summer monsoon rainfall by enhancing the cross-equatorial circulation that brings rainfall to India (Rajagopalan and Molnar, 2013, Vinoj et al., 2014). Goswami et al., (1999) also reported that there is a strong correlation between Hadley circulation and monsoon precipitation.

Figures 9(a)-(c) depict the change in monsoon Hadley cell circulation (averaged over 70ºE-100ºE) obtained from the difference in the Ind38, Ind73 and Chin73 and CTRL simulations. The Ind38 and Chin 73 simulations show a strengthening of the Hadley circulation; a strong ascending branch of the Hadley cell around 10º-20ºN (Fig. 9(a)), whereas the tilted descending branch of Hadley cell is seen over 20ºN in the Ind73 simulation (Fig. 9(b)). In Ind73 simulation ozone heating rates are positive and negative in the vertical direction near ~20ºN (Fig 7 (b)) which might have attributed tilted descending branch of Hadley cell. Consequently, precipitation anomalies over the Indian region (70º-90º E; 8º-35º N) are positive (0.3 to 0.9 mm day^{-1}) in the Ind38 and Chin73 simulations (Figs. 9(d) and 9(f)), whereas they are negative in the Ind73 simulation (-0.3 to -0.6 mm day^{-1}) (Fig. 9(e)). In the upper troposphere (250 hPa-100 hPa), Ind73 simulation shows subsidence while Chin73 simulation shows ascending motion at these levels over the Indian region. Upper tropospheric subsidence in Ind73 simulation might have contributed to the weak positive and negative precipitation anomalies over the North Indian region (Fig. 9(e)). The Chin73 simulation shows subsidence near 22°N below 200 hPa and ascending motion above it. The Chin73 simulation shows ascending motion near 12ºN rising up to 110 hPa, which

338   leads to positive precipitation anomalies over the Indian peninsula.

339   Thus, enhanced Indian (Ind38) and Chinese (Chin73) NO_x emissions increase warming over the

340   Tibetan plateau and enhance precipitation over India via a strengthening of the monsoon Hadley

341   circulation. Remarkably, a further increase of NO_x emissions over India (Ind73) leads to high amounts

342   of ozone in the lower troposphere over the Indo Gangetic plain and Tibetan Plateau. The related ozone

343   heating induces a reversal of the monsoon Hadley circulation, thereby resulting in negative

344   precipitation anomalies.

345   **5. Conclusions**

346   In this paper we investigate the potential impacts of enhanced anthropogenic NO_x emissions on

347   ozone production and distribution during the monsoon season using the state-of-the-art ECHAM5-

348   HAMMOZ model simulations. We performed sensitivity experiments for anthropogenic NO_x

349   enhancements of 38% over India (Ind38 simulation) and 73% over China (Chin73 simulation) in

350   accordance with recently observed trends of 3.8% per year over India and 7.3% per year over China

351   (Ghude et al., 2013; Schneider and van der A., 2012). In another experiment, anthropogenic NO_x

352   emissions over India are increased by 73%, equal to Chinese emissions (Ind73 simulation).

353   These simulations show that an increase in anthropogenic NO_x emissions (over India and

354   China) increases ozone production in the lower and mid-troposphere. The monsoon convection at the

355   southern flank of the Himalayas (80-90°E) and over the Bay of Bengal lifts up the NO_x and ozone

356   anomalies from India across the tropopause into the lower stratosphere. Cross tropopause transport also

357   occurs over China due to convection over the South China Sea.

358   Increase in NO_x emissions in the Ind38, Ind73 and Chin73 simulations leads to increase in

359   ozone radiative forcings, in the anticyclone (15ºN-40ºN, 60ºE-120ºE) of 16.25 mWm^{-2}, 69.88 mW m^{-2},

360   and 78.51 mW m^{-2} in the Ind38, Ind73, and Chin73 simulations, respectively. Enhanced ozone

361   production (Ind38 and Chin73 simulations) increases ozone heating rates which cause anomalous

362   warming over the Tibetan plateau. Further increase in NO_x emissions over the India region (Ind73

363   simulation) produces anomalous heating in the lower troposphere over the Indo Gangetic Plain and

364   Tibetan Plateau. This warming elicits the reversal of the monsoon Hadley cell circulation. The

365   descending branch of the monsoon Hadley circulation over the central India impedes vertical transport

366   of ozone and NO_x anomalies.

367   In the Ind38 and Chin73 simulations, anomalous warming over the Tibetan plateau results in a

368   strengthening of the monsoon Hadley circulation over India and elicits positive precipitation (0.3 to 0.9

369   mm day^{-1}) anomalies over India. However, in Ind73 simulations the reversal of the Hadley circulation

370   and the concurrent subdued warming in the upper troposphere over the Tibetan plateau results in

371   negative precipitation anomalies (-0.3 to -0.6 mm day^{-1}) over India.

372

373   *Acknowledgement:* Dr. S. Fadnavis and C. Roy acknowledges with gratitude Dr. Krishnan, Director of

374   IITM, for his encouragement during the course of this study. We also thank two anonymous reviewers

375   for their valuable suggestions for improvement of this manuscript. Authors acknowledge the High

376   Power Computing Centre (HPC) in IITM, Pune, India, for providing computer resources. Part of the

377   research leading to these results has received funding from the European Community's Seventh

378   Framework Programme (FP7/2007-2013) in the frame of the StratoClim project under grant agreement

379   number 603557. Felix Ploeger was supported by the Helmholtz Young Investigators Group grant A-

380   SPECi (VH-NG-1128).

381

References:

Abad G. G., Allen N. D. C., Bernath P. F., Boone C. D., McLeod S. D., Manney G. L., Toon G. C., Carouge C., Wang Y., Wu S., Barkley M. P., Palmer P. I., Xiao Y., and Fu T. M.: Ethane, ethyne and carbon monoxide concentrations in the upper troposphere and lower stratosphere from ACE and GEOS-Chem: a comparison study, Atmos. Chem. Phys., 11, 9927–9941, 2011. doi:10.5194/acp-11-9927-2011, 2011.

Abhik S., Mukhopadhyay P., Goswami B. N., Evaluation of mean and intraseasonal variability of Indian summer monsoon simulation in ECHAM5: identification of possible source of bias, Climate Dynamics, Volume 43, Issue 1, pp 389–406, 2014.

Barret, B., Sauvage, B., Bennouna, Y., and Le Flochmoen, E.: Upper-tropospheric CO and O_3 budget during the Asian summer monsoon, Atmos. Chem. Phys., 16, 9129-9147, doi:10.5194/acp-16-9129-2016, 2016.

Bekki, S., Rap, A., Poulain, V., Dhomse, S., Marchand, M., Lefevre, F., Forster, P. M., Szopa, S. and Chipperfield, M. P.: Climate impact of stratospheric ozone recovery, Geophys. Res. Lett., 40(11),2796-2800,doi:10.1002/grl.50358,2013.

Bian, J., Pan, L. L., Paulik, L., Vömel, H., Chen, H., and Lu, D.: In situ water vapor and ozone measure-ments in Lhasa and Kunming during the Asian summer monsoon, Geophys. Res. Lett., 39, L19808, doi:10.1029/2012GL052996, 2012.

Braesicke, P., Smith, O. J., Telford, P., & Pyle, J. A.: Ozone concentration changes in the Asian summer monsoon anticyclone and lower stratospheric water vapour: An idealised model study. Geophysical Research Letters, 38(3), doi: 10.1029/2010GL046228, 2011.

Chatani, S., Amann, M., Goel, A., Hao, J., Klimont, Z., Kumar, A., Mishra, A., Sharma, S., Wang, S. X., Wang, Y. X., and Zhao, B.: Photochemical roles of rapid economic growth and potential abatement strategies on tropospheric ozone over South and East Asia in 2030, Atmos. Chem. Phys., 14, 9259-9277, doi:10.5194/acp-14-9259-2014, 2014.

Chen, B., Xu, X., D, Yang, S., and Zhao, T. L.: Climatological perspectives of air transport from atmospheric boundary layer to tropopause layer over Asian monsoon regions during boreal summer inferred from Lagrangian approach, Atmos. Chem. Phys., 12, 5827–5839, doi:10.5194/acp-12-5827-2012. 2012.

Dentener F., Kinne S., Bond T., Boucher O., Cofala J., Generoso S., Ginoux P., Gong S., Hoelzemann J. J., Ito A., Marelli L., Penner J. E., Putaud J.-P., Textor C., Schulz M., Werf G. R. van der, and Wilson J.: Emissions of primary aerosol and precursor gases in the years 2000 and 1750 prescribed data-sets for AeroCom, Atmos. Chem. Phys., 6, 4321-4344, doi:10.5194/acp-6-4321-2006, 2006.

Druyan L. M., Fulakeza M. and Lonergan P.: The impact of vertical resolution on regional model simulation of the west African summer monsoon, Int. J. Climatol. 28: 1293–1314, DOI: 10.1002/joc.1636, 2008.

Edwards, J. M., and Slingo, A.: Studies with a flexible new radiation code .1. Choosing a configuration for a large-scale model, Quart. Jour. Roy. Met. Soc., 122(531), 689-719, doi:10.1002/qj.49712253107,1996.

Fadnavis, S., Semeniuk, K., Pozzoli, L., Schultz, M. G., Ghude, S. D., Das, S., and Kakatkar, R.: Transport of aerosols into the UTLS and their impact on the Asian monsoon region as seen in a global model simulation, Atmos. Chem. Phys., 13, 8771–8786, doi:10.5194/acp-13-8771-2013, 2013.

Fadnavis, S., Semeniuk, K., Schultz, M. G., Kiefer, M., Mahajan, A., Pozzoli, L., and Sonbawane, S.: Transport pathways of peroxyacetyl nitrate in the upper troposphere and lower stratosphere from different monsoon systems during the summer monsoon season. Atmos. Chem. and

429   Phys., 15, doi:10.5194/acp-15-11477-2015, 11477-11499, 2015.

430 Fadnavis, S., Semeniuk, K., Schultz, M. G., Mahajan, A., Pozzoli, L., Sonbawane, S., and Kiefer, M.:
431   Transport pathways of peroxyacetyl nitrate in the upper troposphere and lower stratosphere
432   from different monsoon systems during the summer monsoon season, Atmos. Chem. Phys.
433   Discuss., 14, 20159–20195, doi:10.5194/acpd-14-20159-2014, 2014.

434 Fiore, A. M., Horowitz, L. W., Purves, D. W., Levy II, H., Evans, M. J., Wang, Y., Li, Q., and
435   Yantosca, R. M.: Evaluating the contribution of changes in isoprene emissions to surface ozone
436   trends over the eastern United States, J. Geophys. Res., 110, D12303,
437   doi:10.1029/2004JD005485, 2005.

438 Flohn, H.: Large-scale aspects of the summer monsoon in South and East Asia, J. Meteor. Soc. Japan,
439   75, 180–186, doi: 551.553.21:551.589.5, 1957.

440 Flohn, H.: Recent investigations on the mechanism of the "Summer Monsoon" of Southern and
441   Eastern Asia, Proc. Symp. Monsoon of the World, 1960.

442 Forster, F., Piers, M., and Keith, P. Shine: Radiative forcing and temperature trends from stratospheric
443   ozone changes, J. Geophys Res, 102, 10841-10855, 1997.

444   Froidevaux, L., Livesey, N. J., Read, W. G., Jiang, Y. B., Jimenez, C. J., Filipiak, M. J., Schwartz, M.
445   J., Santee, M. L., Pumphrey, H. C., Jiang, J. H., Wu, D. L., Manney, G. L., Drouin, B. J.,
446   Waters, J. W., Fetzer, E. J., Bernath, P. F., Boone, C. D., Walker, K. A., Jucks, K. W., Toon, G.
447   C., Margitan, J. J., Sen, B., Webster, C. R., Christensen, L. E., Elkins, J. W., Atlas, E., Ueb, R.
448   A., and Hendershot, R.: Early validation analyses of atmospheric profiles from EOS MLS on
449   the Aura satellite. IEEE Trans. Geosci. Remote Sensing 44, 1106 − 1121, doi:
450   10.1109/TGRS.2006.864366, 2006.

451 Fu, R., Hu, Y. L., Wright, J. S., Jiang, J. H., Dickinson, R.E., Chen, M. X., Filipiak, M., Read, W. G,
452   Waters, J. W.,and Wu, D. L.: Short circuit of water vapor and polluted air to the global
453   stratosphere by convective transport over the Tibetan Plateau, P. Natl. Acad. Sci. USA, 103,
454   5664–5669, doi:10.1073/pnas.0601584103, 2006.

455 Ganzeveld, L. and Lelieveld, J.: Dry deposition parameterization in a chemistry general circulation
456   model and its influence on the distribution of reactive trace gases, J. Geophys. Res., 100,
457   20999–21012, doi:10.1029/95JD02266, 1995.

458 Garny, H. and Randel, W. J.: Dynamic variability of the Asian monsoon anticyclone observed in
459   potential vorticity and correlations with tracer distributions, J. Geophys. Res. Atmos., 118,
460   13,421–13,433, doi:10.1002/2013JD020908, 2013.

463 Gettelman, A., Kinnison, D. E., Dunkerton, T. J., and Brasseur, G. P.: Impact of monsoon circulations
464   on the upper troposphere and lower stratosphere, J. Geophys. Res., 109, D22101,
465   doi:10.1029/2004jd004878, 2004.

466 Ghude, S. D., Kulkarni, S. H., Jena, C., Pfister, G. G., Beig, G., Fadnavis, S., and van der A R. J.:
467   Application of satellite observations for identifying regions of dominant sources of nitrogen
468   oxides over the Indian Subcontinent, J. Geophys. Res., 118, 1–15, doi:10.1029/2012JD017811,
469   2013.

470 Goswami, B. N., Krishnamurthy, V., and Annamalai, H.: A broad-scale circulation index for the
471   interannual variability of the Indian summer monsoon. Q. J. R. Meteorol. soc., 125, 611-633,
472   doi: 10.1002/qj.49712555412, 1999.

473 Gu, D., Wang, Y., Smeltzer, C., and Boersma, K. F.: Anthropogenic emissions of NOx over China:
474   Reconciling the difference of inverse modeling results using GOME-2 and OMI
475   measurements, J. Geophys. Res. Atmos., 119, doi:10.1002/ 2014JD021644, 2014.

478 Hilboll, A., Richter, A., and Burrows, J. P.: Long-term changes of tropospheric NO2 over megacities
479   derived from multiple satellite instruments, Atmos. Chem. Phys., 13, 4145–4169,
480   doi:10.5194/acp-13-4145-2013, 2013.

Horowitz, L. W., Walters, S., Mauzerall, D. L., Emmons, L. K., Rasch, P. J., Granier, C., Tie, X., Lamarque, J., Schultz, M. G.,Tyndall, G. S., Orlando, J. J., and Brasseur, G. P.: A global simulation of tropospheric ozone and related tracers, Description and evaluation of MOZART, version 2, J. Geophys. Res., 108, 4784, doi:10.1029/2002JD002853, 2003.

Jacob, D. J., Logan, J. A., and Murti, P. P.: Effect of rising Asian emissions on surface ozone in the United States, Geophys. Res. Lett., 26, 2175–2178, doi:10.1029/1999GL900450, 1999.

Kärcher B. and U. Lohmann, A parameterization of cirrus cloud formation: Homogeneous freezing of supercooled aerosols, J. Geophy. Res. 107, NO. D2, 4010, 10.1029/2001JD000470, 2002.

Konopka, P., Grooß, J.U., Günther, G., Ploeger, F., Pommrich, R., Müller, R. and Livesey, N.: Annual cycle of ozone at and above the tropical tropopause: observations versus simulations with the Chemical Lagrangian Model of the Stratosphere (CLaMS), Atmos. Chem. Phys., 10(1), 121-132, doi: www.atmos-chem-phys.net/10/121/2010/, 2010.

Kunze, M., Braesicke, P., Langematz, U., Stiller, G., Bekki, S., Brühl, C., Chipperfield, M., Dameris, M., Garcia, R. and Giorgetta, M.: Influences of the Indian summer monsoon on water vapor and ozone concentrations in the UTLS as simulated by chemistry-climate models, J. Clim., 23(13), 3525-3544, doi: http://dx.doi.org/10.1175/2010JCLI3280.1, 2010.

Lacis Andrew, A., Donald Wuebbles, J., and Jennifer Logan A., Radiative Forcing of climate by Changes in the Vertical Distribution of Ozone, J. Geophys. Res., 95 , 9971-9981, doi: 10.1029/JD095iD07p09971, 1990.

Lawrence, M. G.: Atmospheric science: Asia under a high-level brown cloud, Nat. Geosci., 4, 352–353, doi:10.1038/ngeo1166, 2011.

Lei, W., Zhang, R., Tie, X., and Hess, P.: Chemical characterization of ozone formation in the Houston-Galveston area. J.Geophys.Res., 109, doi: 10.1029/2003JD004219, 2004.

Li, C. and Yanai M.: The onset and interannual variability of the Asian summer monsoon in relation to land–sea thermal contrast, J. Clim. 9: 358–375, doi: http://dx.doi.org/10.1175/1520-0442(1996)009<0358:TOAIVO>2.0.CO;2, 1996.

Li, Q., Jiang, J. H., Wu, D. L., Read, W. G., Livesey, N. J., Waters, J. W., Zhang, Y., Wang, B.,. Filipiak, M. J, Davis, C. P., Turquety, S., Wu, S., Park, R. J., Yantosca, R. M., and Jacob, D. J.: Convective outflow of south Asian pollution: a global CTM simulation compared with EOS MLS observations, Geophys. Res. Lett., 32, doi: http://dx.doi.org/10.1029/2005GL022762, doi: 10.1029/2005GL022762, 2005.

Livesey, N. J., Read, W. G., Filipiak, M. J., Froidevaux, L., Harwood, R. S., Jiang, J. H., Jimenez, C., Pickett, H. M., Pumphrey, H. C., Santee, M. L., Schwartz, M. J., Waters, J. W., and Wu, D. L.: EOS MLS Version 1.5 Level 2 data quality and description document, JPL, California, 2005.

Livesey, N. J., Read, W. G., Froideveaux, L., Lambert, A., Manney, G. L., Pumphrey, H. C., Santee, M. L., Schwartz, M. J., Wang, S., Cofield, R. E., Cuddy, D. T., Fuller, R. A., Jarnot, R. F., Jiang, J. H., Knosp, B. W., Stek, P. C., Wagner, P. A., and Wu, D. L.: Version 3.3 Level 2 data quality and description document. Tech Rep. JPL D-33509, Jet Propulsion Laboratory, available at: http://mls.jpl.nasa.gov (last access: 17 August 2015), 2011.

Lohmann, U., J. Feichter, C. C. Chuang, and J. E. Penner, Predicting the number of cloud droplets in the ECHAM GCM, J. Geophys. Res., 104, 9169 – 9198, 1999.

Meehl, G. A.: Coupled land-ocean-atmosphere processes and South Asian monsoon variability, Science, 266, 263–267, doi: 10.1126/science.266.5183.263, 1994.

Myhre, G., et al., Anthropogenic and natural radiative forcing, in Climate Change 2013: The Physical Science Basis. Contribution of Working Group I to the Fifth Assessment Report of the Intergovernmental Panel on Climate Change, edited by T. F. Stocker et al., pp. 659–740, Cambridge Univ. Press, Cambridge, U. K., and New York, 2013.

Park, M., Randel, W. J., Emmons, L. K., Bernath, P. F., Walker, K. A., and Boone, C. D.: Chemical

isolation in the Asian monsoon anticyclone observed in Atmospheric Chemistry Experiment (ACE-FTS) data, Atmos. Chem. Phys., 8, 3, 757-764, doi: www.atmos-chem-phys.net/8/757/2008/, 2008.

Park, M., Randel, W. J., Emmons, L. K., and Livesey, N. J.:Transport pathways of carbon monoxide in the Asian summer monsoon diagnosed from Model of Ozone and Related Tracers (MOZART), J. Geophys. Res., 114, D08303, doi:10.1029/2008jd010621, 2009.

Park, M., Randel, W. J., Gettelman, A., Massie, S. T., and Jiang, J.H.: Transport above the Asian summer monsoon anticyclone inferred from Aura Microwave Limb Sounder tracers, J. Geophys.Res., 112, D16309,doi:10.1029/2006jd008294, 2007.

Park, M., Randel, W. J., Kinnison, D. E., Garcia, R. R., and Choi, W.: Seasonal variation of methane, water vapour, and nitrogen oxides near the tropopause: Satellite observations and model simulations, J. Geophys. Res., 109, D03302, doi:10.1029/2003JD003706, 2004.

Penki, R. K. and Kamra, A. K.: Lightning distribution with respect to the monsoon trough position during the Indian summer monsoon season, J. Geophy. Res., 118, 4780–4787, doi:10.1002/jgrd.50382, 2013.

Ploeger, F., Gottschling, C., Griessbach, S., Grooß, J.-U., Guenther, G., Konopka, P., Müller, R., Riese, M., Stroh, F., Tao, M., Ungermann, J., Vogel, B., and von Hobe, M.: A potential vorticity-based determination of the transport barrier in the Asian summer monsoon anticyclone, Atmos. Chem. Phys., 15, 13145-13159, doi:10.5194/acp-15-13145-2015, 2015.

Pozzoli, L., Bey, I., Rast, J. S., Schultz, M. G., Stier, P., and Feichter, J.: Trace gas and aerosol interactions in the fully coupled model of aerosol-chemistry-climate ECHAM5- HAMMOZ: 1. Model description and insights from the spring 2001 TRACE-P experiment, J. Geophys. Res., 113, D07308, doi:10.1029/2007JD009007, 2008a.

Pozzoli, L., Bey, I., Rast, J. S., Schultz, M. G., Stier, P., and Feichter, J.: Trace gas and aerosol interactions in the fully coupled model of aerosol-chemistry-climate ECHAM5- HAMMOZ: 2. Impact of heterogeneous chemistry on the global aerosol distributions, J. Geophys. Res., 113, D07309, doi:10.1029/2007JD009008, 2008b.

Pozzoli, L., Janssens-Maenhout, G, Diehl, T., Bey, I., Schultz, M. G., Feichter, J., Vignati, E., and Dentener, F.: Re-analysis of tropospheric sulfate aerosol and ozone for the period 1980–2005 using the aerosol-chemistry-climate model ECHAM5-HAMMOZ, Atmos. Chem. Phys., 11, 9563–9594, doi:10.5194/acp-11-9563-2011, 2011.

Rajeevan M., Bhate J.,. Kale J.D and Lal B.:Development of High Resolution Daily Gridded Rainfall Data for the Indian Region, Met. Monograph Climatology No. 22/2005, National Climate Centre India Meteorological Department. Pune 411 005, India, 2005.

Rajagopalan, B., and Molnar, P.: Signatures of Tibetan Plateau heating on Indian summer monsoon rainfall variability, J. Geophys. Res. Atmos., 118, 1170–1178, doi:10.1002/jgrd.50124, 2013.

Ranalkar, M. R. and Chaudhari, H. S.: Seasonal variation of lightning activity over the Indian subcontinent, Meteorol. Atmos.Phys., 104, 125–134, doi: 10.1007/s00703-009-0026-7, 2009.

Randel, W. J., and Park M.: Deep convective influence on the Asian summer monsoon anticyclone and associated tracer variability observed with Atmospheric Infrared Sounder (AIRS), J. Geophys. Res.,111, D12314, doi:10.1029/2005JD006490, 2006.

Randel, W. J., Park, M., Emmons, L., Kinnison, D., Bernath, P., Kaley Walker, A., Boone, C., and Pumphrey, H.: Asian Monsoon Transport of Pollution to the Stratosphere Science, 328(5978), 611-613, doi: 10.1126/science.1182274, 2010.

Randel, W. J., Wu, F., Gettelman, A., Russell, J. M., Jawodny, J. M., and Oltmans, S. J.: Seasonal variation of water vapor in the lower stratosphere observed in Halogen Occultation Experiment data, J. Geo-phys. Res., 106, 14,313 − 14,325, doi: 0148-0227/01/2001JD900048509.00, 2001.

Rap, A., Richards, N., A., D., Forster, P., M., Monks, S., Arnold, S., R., Chipperfield, M.: Satellite

constraint on the tropospheric ozone radiative effect, Geophys. Res. Lett, 42, 5074-5081.doi:10.1002/2015GL064037, 2015.

Revell, L. E., Tummon, F., Stenke, A., Sukhodolov, T., Coulon, A., Rozanov, E., Garny, H., Grewe, V., and Peter, T.: Drivers of the tropospheric ozone budget throughout the 21st century under the medium-high climate scenario RCP 6.0, Atmos. Chem. Phys., 15, 5887-5902, doi:10.5194/acp-15-5887-2015, 2015.

Richter, A., John Burrows, P., Hendrik, N., Granier C., and Niemeier, U.: Increase in tropospheric nitrogen dioxide over China observed from space; 437, doi:10.1038/nature04092, 2005.

Riese, M., Ploeger, F., Rap, A., Vogel, B., Konopka, P., Dameris, M. and Forster, P.: Impact of uncertainties in atmospheric mixing on simulated UTLS composition and related radiative effects, J. Geophys. Res.: Atmos., 117(D16), doi: 10.1029/2012JD017751, 2012.

Rodwell, M. J. and Hoskins, B. J.: Monsoons and the dynamics of deserts, QJRMS, 122(534), 1385-1404, doi: 10.1002/qj.49712253408, 1995.

Roeckner, E., Bauml, G., Bonaventura, L., Brokopf, R., Esch, M., Giorgetta, M., Hagemann, S., Kirchner, I., Kornblueh, L., Manzini, E., Rhodin, A., Schlese, U., Schulzweida, U., and Tompkins, A.: The atmospehric general circulation model ECHAM5: Part 1, Tech. Rep. 349, Max Planck Institute for Meteorology,Hamburg, 2003.

Sander, S. P., Fried, R. R., Barker, J. R., Golden, D. M., Kurylo, M. J.,Wine, P. H., J. Abbatt, P. D., 25 Burkholder, J. B., Kolb, C. E., Moortgat, G. K., Huie, R. E., and Orkin, V. L.: Chemical kinetics and photochemical data for use in atmospheric studies, evaluation number 14, JPL Publ. 02-25, Jet Propul. Lab., Calif. Inst. Of Technol., Pasadena, available at: http://jpldataeval.jpl.nasa.gov/pdf/JPL_02-25_rev02.pdf, 2003.

Schneider, P. and van der A. R. J.: A global single-sensor analysis of 2002–2011 tropospheric nitrogen dioxide trends observed from space, J., Geophy. Res., 117, D16309, doi:10.1029/2012JD017571, 2012.

Schoeberl, M. R., Duncan, B. N., Douglass, A. R., Waters, J., Livesey, N., Read, W., and Filipiak, M.: The carbon monoxide tape recorder. Geophys. Res. Lett., 33(12), doi: 10.1029/2006GL026178, 2006.

Schultz, M. G., Heil, A., Hoelzemann, J. J., Spessa, A., Thonicke, K., Goldammer, J. G., Held, A. C., Pereira, J. M. C., and van het Bolscher, M.: Global wildland fire emissions from 1960 to 2000, Global Biogeochem. Cy., 22, GB2002, doi:10.1029/2007GB003031, 2008.

Schultz, M., Backman, L., Balkanski, Y., Bjoerndalsaeter, S., Brand, R., Burrows, J., Dalsoeren, S., de Vasconcelos, M., Grodtmann, B., Hauglustaine, D., Heil, A., Hoelzemann, J., Isaksen, I., Kaurola, J., Knorr, W., Ladstaetter-Weienmayer, A., Mota, B., Oom, D., Pacyna, J., Panasiuk, D., Pereira, J., Pulles, T., Pyle, J., Rast, S., Richter, A., Savage, N., Schnadt, C., Schulz, M., Spessa, A., Staehelin, J., Sundet, J., Szopa, S., Thonicke, K., van het Bolscher, M., van Noije, T., van Velthoven, P., Vik, A. and Wittrock, F.: REanalysis of the TROpospheric chemical composition over the past 40 years (RETRO). A long-term global modeling study of tropospheric chemistry. Final Report, Tech. rep., Max Planck Institute for Meteorology, Hamburg, Germany, 2007.

Schultz, M.G., Heil A., Hoelzemann, J. J., Spessa, A., Thonicke, K., Goldammer, J.,. Held, A.C, Pereira, J. M., Van Het Bolscher, M.: Global Wildland Fire Emissions from 1960 to 2000, doi:10.1029/2007GB003031 , Global Biogeochemical Cycles 22 (GB2002) : 17 PP, 2005

Sillman, S.: The use of NOy, H_2O_2, and HNO_3 as indicators for ozone-NO_x-hydrocarbon sensitivity in urban locations. J. Geophys. Res., 100, 14,175–14,188, doi: 10.1029/94JD02953, 1995.

Sinha, V., Kumar, V., and Sarkar, C.: Chemical composition of pre-monsoon air in the Indo-Gangetic Plain measured using a new air quality facility and PTR-MS: high surface ozone and strong influence of biomass burning, Atmos. Chem. Phys., 14, 5921–5941, 2014. doi:10.5194/acp-14-

5921-2014, 2014.

Søvde, O. A., Hoyle, C. R., Myhre, G., and Isaksen, I. S. A.: The HNO3 forming branch of the HO2 + NO reaction: pre-industrial-to-present trends in atmospheric species and radiative forcings, Atmos. Chem. Phys., 11, 8929–8943, 2011; doi:10.5194/acp-11-8929-2011, 2011.

Stevenson, D. S., P. J. Young, Vaishali, N., Lamarque, J. F., Drew, T., Shindell, Voulgarakis, A., and Skeie R. B.: Tropospheric ozone changes, radiative forcing and attribution to emissions in the Atmospheric Chemistry and Climate Model Intercomparison Project (ACCMIP), Atmos. Chem. Phys., 13, 3063-3085, doi:10.5194/acp-13-3063-2013, 2013.

Stier, P., Feichter, J., Kinne, S., Kloster, S., Vignati, E., Wilson, J., Ganzeveld, L., Tegen, I., Werner, M., Balkanski, Y., Schulz, M., Boucher, O., Minikin, A., and Petzold, A.: The aerosol-climate model ECHAM5-HAM, Atmos. Chem. Phys., 5, 1125–1156, doi:10.5194/acp-5-1125-2005, 2005.

Thuburn, J. and Craig, G.C.: On the temperature structure of the tropical substratosphere, Journal of Geophysical Research: Atmospheres, 107(D2), doi: 10.1029/2001JD000448, 2002.

Tie, X. X., Zhang, R., Brasseur, G., Emmons, L., and Lei, W.:Effects of lightning on reactive nitrogen and nitrogen reservoir species in the troposphere, J. Geophys. Res.-Atmos., 106, 3167– 3178, doi:10.1029/2000JD900565, 2001.

Tie, X., Madronich, S., Li, G.H., Ying, Z.M., Zhang, R., Garcia, A., Lee-Taylor, and J., Y. Liu. Characterizations of chemical oxidants in Mexico City: a regional chemical/dynamical model (WRF-Chem) study, Atmos. Environ., 41, 1989–2008, doi:10.1016/j.atmosenv.2006.10.053, 2007.

Tiedtke, M.: A comprehensive mass flux scheme for cumulus parameterization in large-scale models, Mon. Weather Rev., 117(8), 1779–1800, 1989.

Tobo, Y., Iwasaka, Y., Zhang, D., Shi, G., Kim, Y. S., Tamura, K., and Ohashi, T.: Summertime ''ozone valley'' over the Tibetan Plateau derived from ozonesondes and EP/TOMS data, Geophys. Res. Lett., 35, L16801, doi:10.1029/2008GL03434, 2008.

Vernier, J.-P., T. D. Fairlie, M. Natarajan, F. G. Wienhold, J. Bian, B. G. Martinsson, S. Crumeyrolle, L. W. Thomason, and Bedka, K.: Increase in upper tropospheric and lower stratospheric aerosol levels and its potential connection with Asian Pollution, J. Geophys. Res. Atmos., 120, 1608–1619, doi:10.1002/2014JD022372, 2015.

Vinoj, V., Rasch, P.J., Wang, H., Yoon, J.H., Ma, P.L., Landu, K. and Singh, B.: Short-term modulation of Indian summer monsoon rainfall by West Asian dust, Nature Geoscience, 7(4), 308-313, doi:10.1038/ngeo2107, 2014.

Vogel B., Günther G., Müller R., Grooß, and Riese M.: Impact of different Asian source regions on the composition of the Asian J.-u. monsoon anticyclone and of the extratropical lowermost stratosphere, Atmos. Chem. Phys., 15, 13699–13716, doi:10.5194/acp-15-13699-2015, 2015.

Vogel, B., Günther, G., Müller, R., Grooß, J.-U., Afchine, A., Bozem, H., Hoor, P., Krämer, M., Müller, S., Riese, M., Rolf, C., Spelten, N., Stiller, G. P., Ungermann, J., and Zahn, A.: Long-range transport pathways of tropospheric source gases originating in Asia into the northern lower stratosphere during the Asian monsoon season 2012, Atmos. Chem. Phys. Discuss., doi:10.5194/acp-2016-463, revised paper accepted for ACPD, 2016.

Waters, J. W., Froidevaux, L., Harwood, R.S., Jarnot, R.F., Pickett, H. M., Read, W. G., Siegel, P. H., Cofield, R. E., Filipiak, M. J., Flower, D. A., Holden, J. R., Lau, G. K., Livesey, N. J., Manney, G. L., Pumphrey, H. C., Santee, M. L., Wu, D. L., Cuddy, D. T., Lay, R. R., Loo, M. S., Perun, V. S., Schwartz, M. J., Stek, P. C., Thurstans, R. P., Boyles, M. A., Chandra, S., Chavez, M. C., Chen, G. S., Chudasama, B. V., Dodge, R., Fuller, R. A., Girard, M.A., Jiang, J. H., Jiang, Y., Knosp, B. W., LaBelle, R. C., Lee, K. A., Miller, D., Oswald, J. E., Patel, N. C., Pukala, D. M., Quintero, O., Scaff, D. M., Snyder, W. V., Tope, M. C., Wagner, P. A., and Walch, M. J.:

679    The Earth Observing System Microwave LimbSounder (EOS MLS) on the Aura satellite.
680     IEEE Trans, Geosci., Remote Sensing, 44, 1075 – 1092, doi: 10.1109/TGRS.2006.873771,
681     2006.
682 Wild, O., and Akimoto, H.: Intercontinental transport of ozone and its precursors in a three-
683     dimensional global CTM, J., Geophys. Res., 106(D21), 27729-27744, doi:
684     http://dx.doi.org/10.1029/2000JD000123, 2001.
685 Wu, G. X., and Zhang, Y. S.: Tibetan Plateau forcing and the timing of the monsoon onset over South
686     Asia and the South China Sea, Mon Wea Rev 126:913–927, doi:
687     http://dx.doi.org/10.1175/1520-0493(1998)126<0913:TPFATT>2.0.CO;2, 1998.
688 Xiong, X., Houweling S., Wei J., Maddy E., Sun F., and Barnet C.: Methane plume over south Asia
689     during the monsoon season: satellite observation and model simulation, Atmos. Chem. Phys.,
690     9, 783–794, doi:10.5194/acp-9-783-2009, 2009.
691 Yamaji, K., T. Ohara, I. Uno, H. Tanimoto, J. Kurokawa, and Akimoto H.: Analysis of the seasonal
692     variation of ozone in the boundary layer in East Asia using the Community Multiscale Air
693     Quality model: what controls surface ozone levels over Japan?, Atmos. Environ., 40, 1856–
694     1868, 2006.
695 Yanai, M., Li, C., Song, Z.: Seasonal heating of the Tibetan Plateau and its effects on the evolution of
696     the Asian summer monsoon, J Meteor Soc Japan, 70, 189–221, 1992.
697 Zhang, R.W., Lei, X., and Hess, T. P.: Industrial emissions cause extreme diurnal urban ozone
698     variability. Proc. Natl. Acad. Sci., 101, 6346–6350, doi: 10.1073/pnas.0401484101, 2004.
699 Zhao, B., Wang, S. X., Liu, H., Xu, J. Y., Fu, K., Klimont, Z., Hao, J. M., He, K. B., Cofala, J., and
700     Amann, M.: NOx emissions in China: historical trends and future perspectives, Atmos. Chem.
701     Phys., 13, 9869–9897, doi:10.5194/acp-13-9869-2013, 2013.

702

703   Table 1: Details of the sensitivity experiments (2000 - 2010).

704

Name of experiment	Prescribed SSTs	Emissions
CTRL	AMIP2 SST and SIC varying from 2000 – 2010	RETRO anthropogenic NO_x emissions for the year 2000.
Ind38	AMIP2 SST and SIC varying from 2000 – 2010	RETRO anthropogenic NO_x emissions for the year 2000 are increased by 38% over India for 11 years period 2000-2010
Chin73	AMIP2 SST and SIC varying from 2000 – 2010	RETRO anthropogenic NO_x emissions for the year 2000 are increased by 73% over China for 10 years period 2000-2010.
Ind73	AMIP2 SST and SIC varying from 2000 – 2010	RETRO anthropogenic NO_x emissions for the year 2000 are increased by 73% over India for 10 years period 2000-2010.
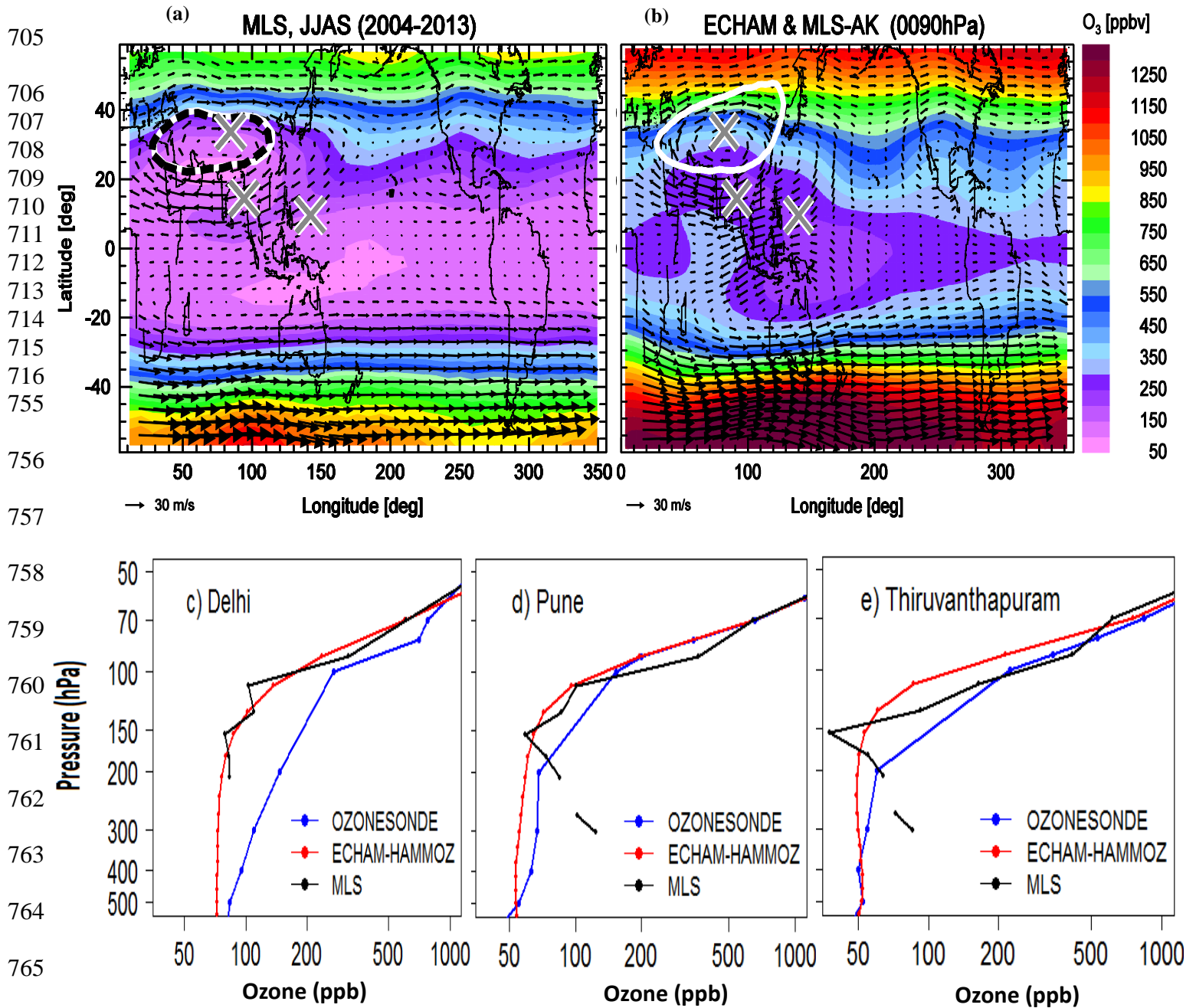
Figure 1: Distribution of ozone mixing ratio (ppb) during the monsoon season (June-September) obtained from (a) MLS observations at 100 hPa, and (b) from ECHAM-HAMMOZ at 90hPa. Black arrows indicate wind vectors, the black dashed contour shows the PV-gradient based transport barrier of the anticyclone (calculated following Ploeger et al., 2015), and the white contour shows the 270m geopotential height anomaly, corresponding to the anticyclone edge definition by Barret et al. (2016) (Meteorological data shows climatological July fields from ERA-Interim reanalysis (a) ERA-Interim

reanalysis and (b) ECHAM5-HAMMOZ. The ECHAM5-HAMMOZ ozone distribution is smoothed using the MLS averaging kernel. Grey crosses highlight the regions of the Tibetan plateau, Bay of Bengal and South China Sea. Bottom panels show the vertical distribution of seasonal (June-September) mean ozone mixing ratios (ppb) from ozonesonde (2001-2009), MLS (2004-2013) and ECHAM5-HAMMOZ CTRL simulation at the (c) Delhi, (d) Pune, and (e) Thiruvananthpuram Indian stations.
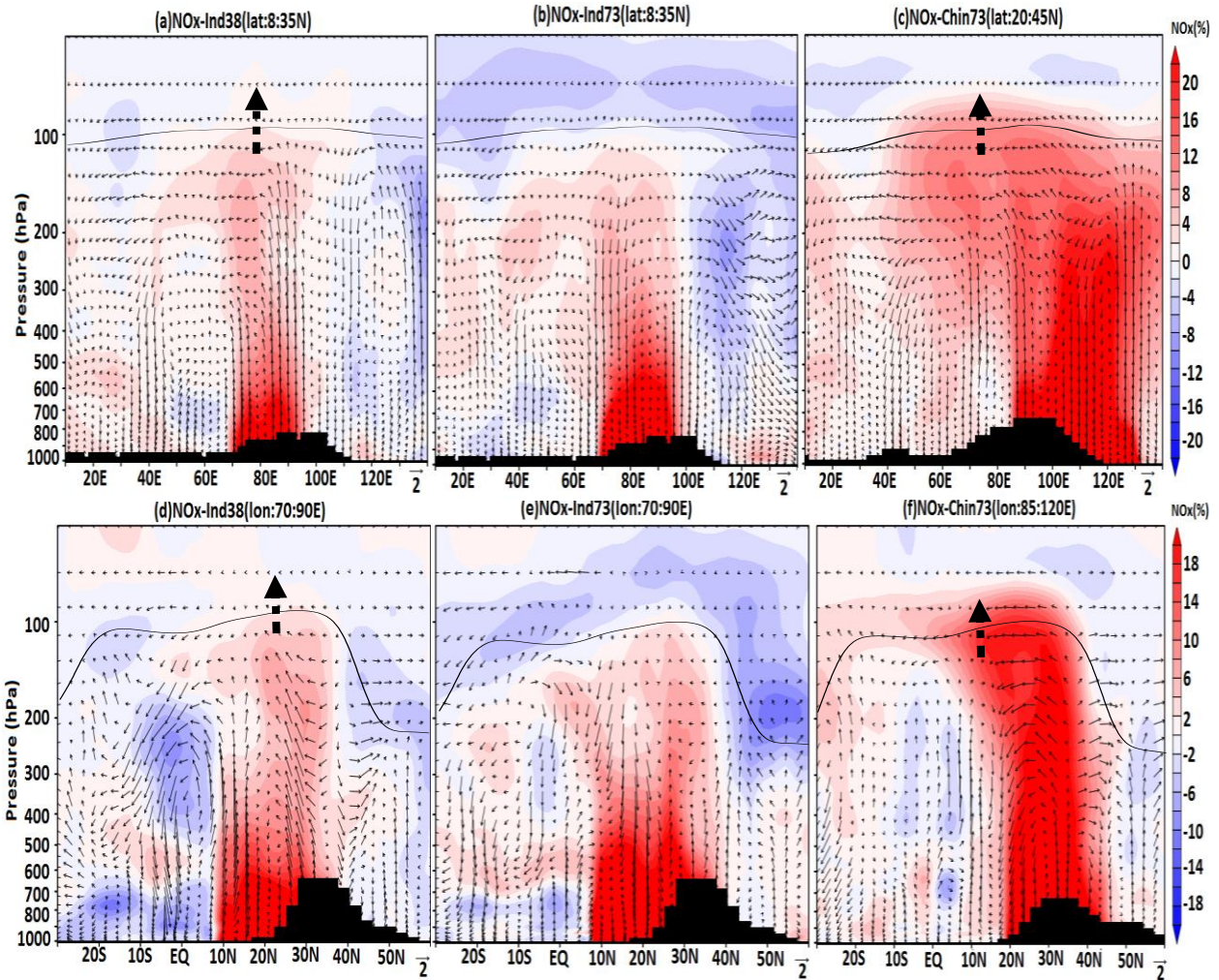
Figure 2: Longitude pressure cross-sections of percentage NO$_x$ anomalies averaged for the monsoon season (June-September) obtained from (a) Ind38 (averaged over 8ºN-35ºN), (b) Ind73 (averaged over 8ºN-35ºN), and (c) Chin73 (averaged over 20ºN-45ºN) simulations. Latitude pressure cross-sections of percentage NO$_x$ anomalies averaged for the monsoon season (June-September) obtained from (d) Ind38 (averaged over 70ºE-90ºE), (e) Ind73 (averaged over 70ºE-90ºE), and (f) Chin73 (averaged over 85ºE-120ºE) simulations. Black arrows indicate wind vectors (the vertical velocity field has been scaled by 300), the black line represents the tropopause, and the black dashed arrows indicate the cross tropopause transport.

804

Figure 3: Longitude pressure cross-section of changes in net ozone production (ppt/day) due to enhanced NO$_x$ with respect to the CTRL simulation, averaged for the monsoon season (June-September) obtained from (a) Ind38 (averaged over 8ºN-35ºN), (b) Ind73 (averaged over 8ºN-35ºN), and (c) Chin73 (over 20ºN-45ºN) simulations. The black line shows the tropopause while black contours indicate 95% confidence level.
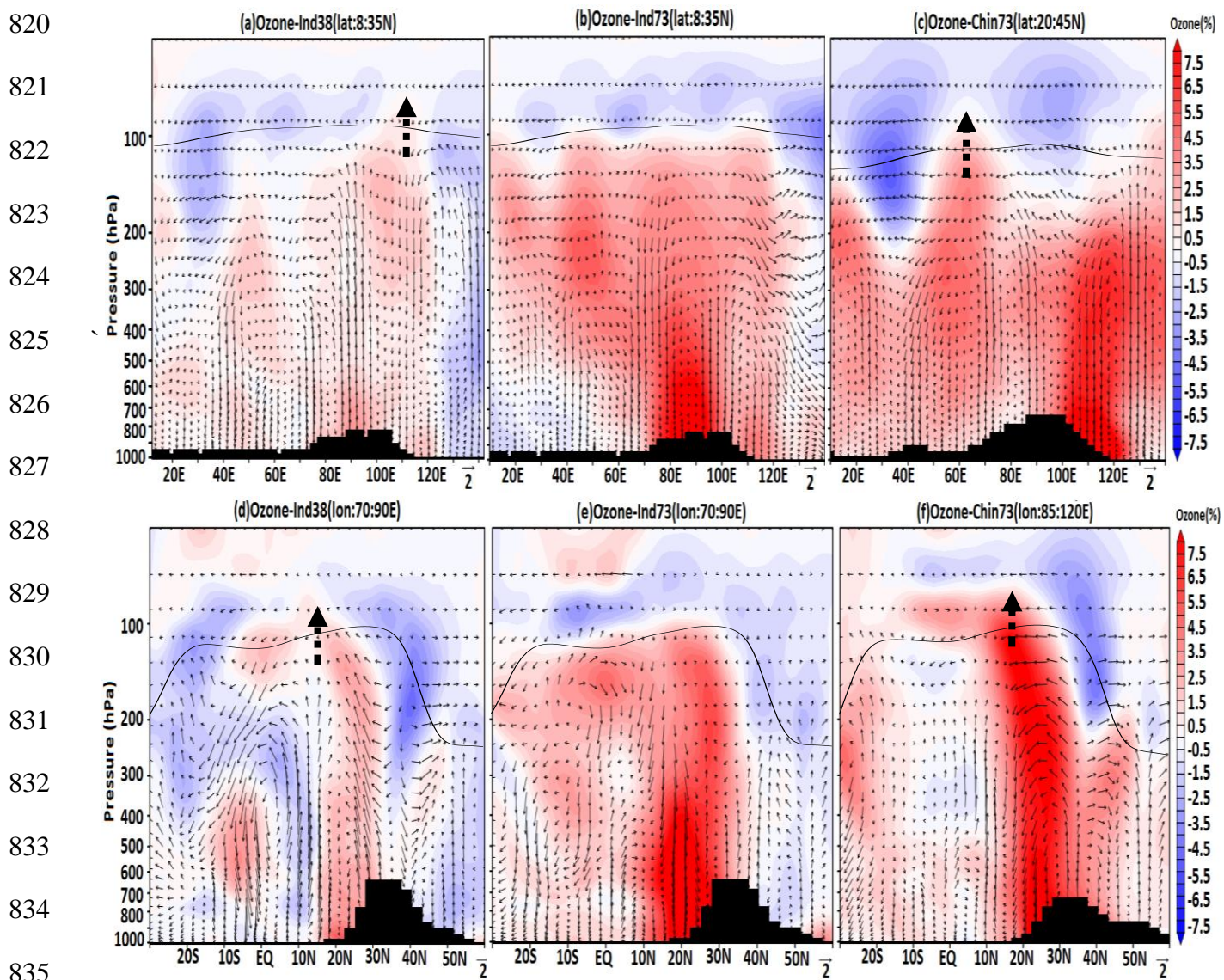
Figure 4: Longitude pressure cross-section of percentage ozone anomalies averaged for the monsoon season (June-September) obtained from (a) Ind38 (averaged over 8ºN-35ºN), (b) Ind73 (averaged over 8ºN-35ºN), and (c) Chin73 (averaged over 20ºN-45ºN) simulations. Latitude pressure cross-section of percentage ozone anomalies averaged for the monsoon season (June-September) obtained from (d) Ind38 (averaged over 70ºE-90ºE), (e) Ind73 (averaged over 70ºE-90ºE), and (f) Chin73 (averaged over 85ºE-120ºE) simulations. Black arrows indicate wind vectors. The vertical velocity field has been scaled by 300. The black line represents the tropopause, and the black dashed arrows indicate the cross tropopause transport.

Figure 5: Latitude-longitude cross-section of percentage NO_x anomalies averaged for the monsoon season (June-September) at 110 hPa obtained from (a) Ind38, (b) Ind73, and (c) Chin73 simulations. Panels (d-f) show the same but for percentage ozone anomalies at 110 hPa for the (d) Ind38, (e) Ind73, and (f) Chin73 simulations. Black arrows indicate horizontal winds at 110 hPa. The red box in panel (a) indicates the ASM anticyclone region used to compute the associated radiative forcing regional average.

861

862

863

864

865

866

867

868

869

870 Figure 6: Latitude-longitude distribution of changes in ozone radiative forcing (in mW m^{-2}) for the (a)

871 Ind38, (b) Ind73, and (c) Chin73 perturbed simulations, compared to the CTRL simulation.
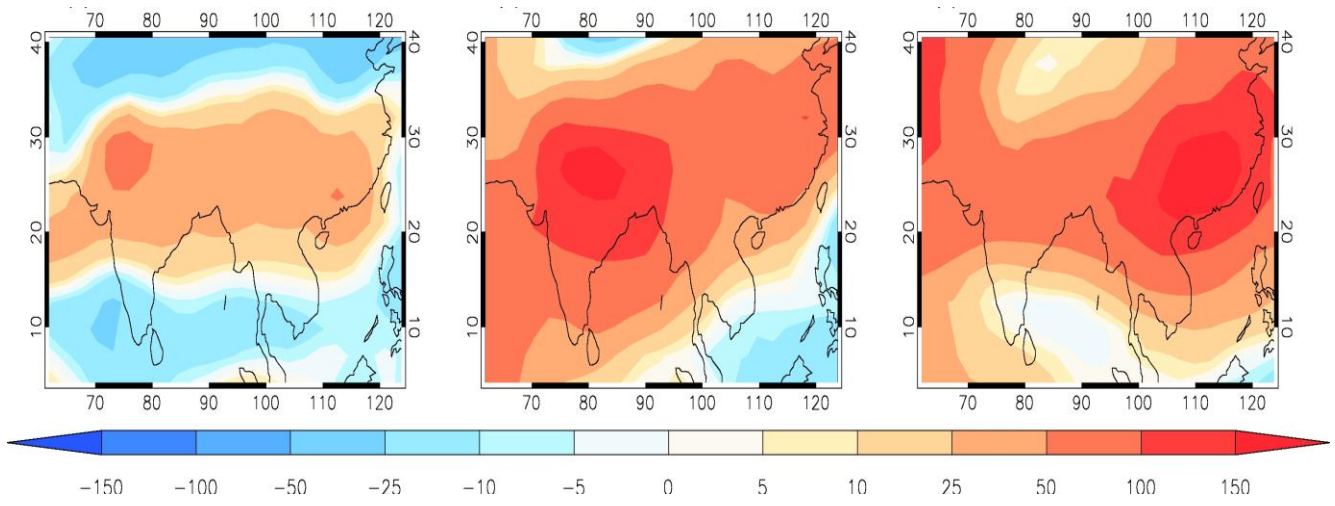
872

873

874

875

876

877

878

879

880

881

882

883   Figure 7: Latitude- pressure distribution of ozone heating rate changes (in K/day) for the (a) Ind38

884   (averaged over 70º-100ºE), (b) Ind73 (averaged 70º-100ºE), and (c) Chin73 (averaged over 90º -100º

885   E) perturbed simulations, compared to the CTRL simulation.
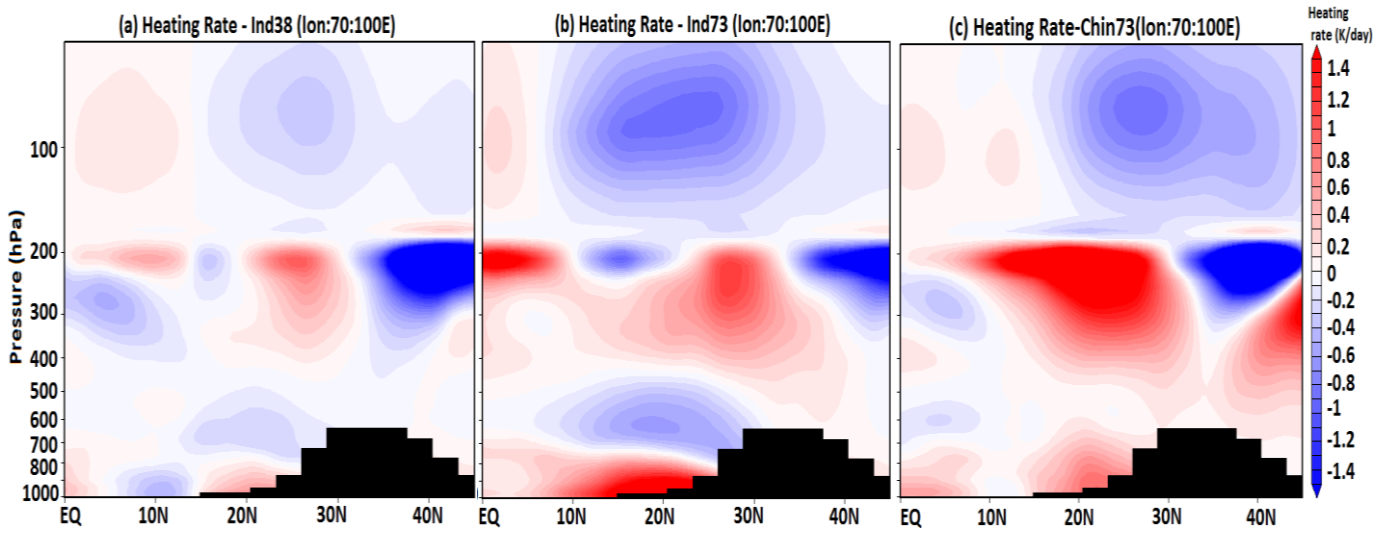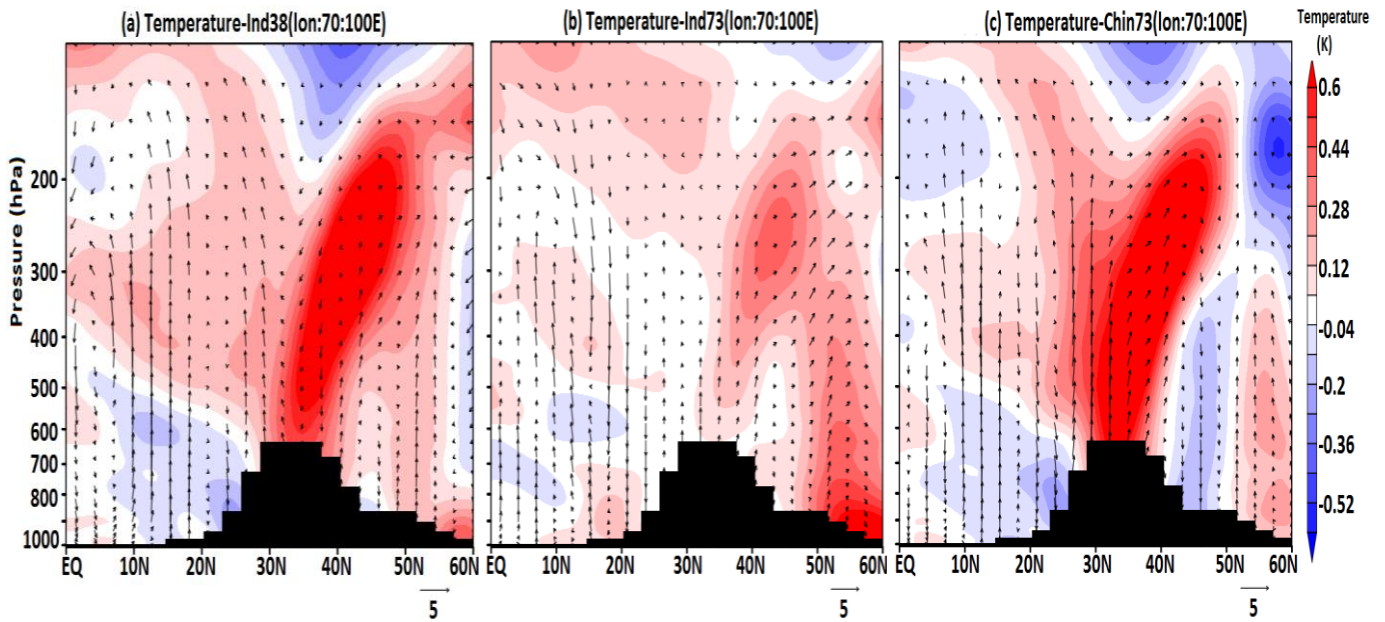
Figure 8: Latitude pressure cross-section of temperature anomalies (K) averaged for the monsoon season (June-September) and over 70ºE-100ºE obtained from (a) Ind38-CTRL, (b) Ind73-CTRL, and (c) Chin73-CTRL simulations. Black arrows indicate wind vectors (the vertical velocity field has been scaled by 300).
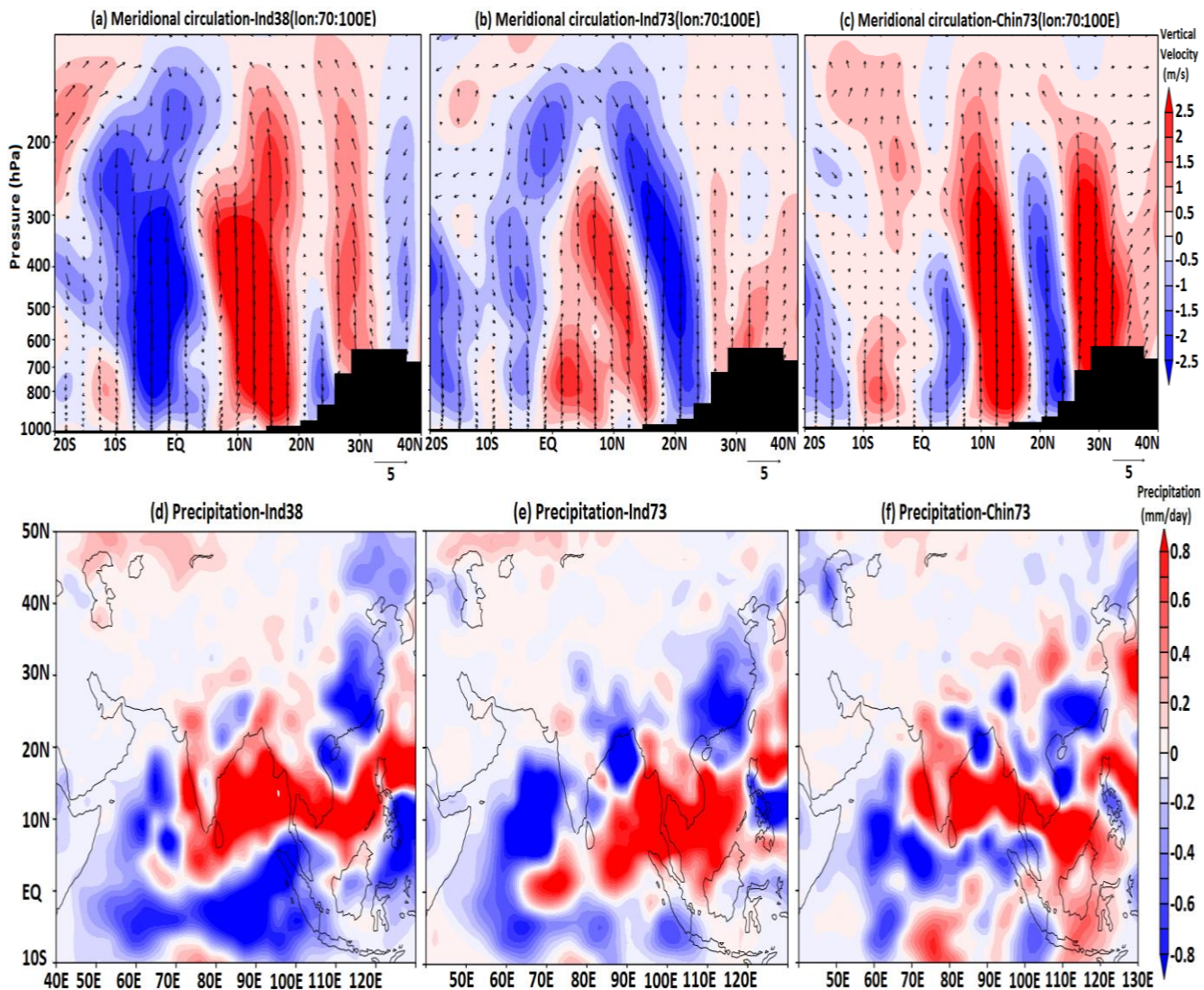
Figure 9: Difference in the meridional circulation due to enhanced NO$_X$ emissions averaged for the monsoon season (June-September) and over 70ºE-110ºE for (a) Ind38-CTRL (b) Ind73-CTRL (c) Chin73-CTRL simulations. Shaded contours indicate the anomalies in vertical velocity (m/s). The vertical velocity field has been scaled by 300. Precipitation anomalies (mm/day) averaged for the monsoon season (June-September) obtained from (d) India38-CTRL (e) Ind73-CTRL, and (f) Chin73-CRTL simulations.